ACS NANO
Cite This: ACS Nano 2019, 13, 1097−1106
www.acsnano.org

ARTICLE

# Exfoliated Graphene Leads to Exceptional Mechanical Properties of Polymer Composite Films

Yunsong Pang,[†,¶] Junlong Yang,[‡,¶] Tyler E. Curtis,[†] Shirui Luo,[†,§] Dezhao Huang,[†] Zhe Feng,[†] Jorge O. Morales-Ferreiro,[†,∥] Pitambar Sapkota,[⊥] Fan Lei,[‡] Jianming Zhang,[‡,#] Qinnan Zhang,[▽] Eungkyu Lee,[†] Yajiang Huang,[○] Ruilan Guo,[▽] Sylwia Ptasinska,[⊥] Ryan K. Roeder,[†] and Tengfei Luo*[,†,▽,◆]

[†]Department of Aerospace and Mechanical Engineering, University of Notre Dame, Notre Dame, Indiana 46556, United States
[‡]Department of Materials Science and Engineering, Southern University of Science and Technology, Shenzhen 518055, P. R. China
[§]National Center for Supercomputing Applications, University of Illinois at Urbana−Champaign, Urbana, Illinois 61801, United States
[∥]Facultad de Ingeniería, Universidad de Talca, Camino los Niches Km1, Curico 3340000, Chile
[⊥]Radiation Laboratory and Department of Physics, University of Notre Dame, Notre Dame, Indiana 46556, United States
[#]Academy for Advanced Interdisciplinary Studies, Southern University of Science and Technology, Shenzhen 518055, P. R. China
[▽]Department of Chemical and Biomolecular Engineering, University of Notre Dame, Notre Dame, Indiana 46556, United States
[○]College of Polymer Science and Engineering, State Key Laboratory of Polymer Materials Engineering of China, Sichuan University, Chengdu 610065, P. R. China
[◆]Center for Sustainable Energy at Notre Dame, Notre Dame, Indiana 46556, United States

Supporting Information

**ABSTRACT:** **Polymers with superior mechanical properties are desirable in many applications. In this work, polyethylene (PE) films reinforced with exfoliated thermally reduced graphene oxide (TrGO) fabricated using a roll-to-roll hot-drawing process are shown to have outstanding mechanical properties. The specific ultimate tensile strength and Young's modulus of PE/TrGO films increased monotonically with the drawing ratio and TrGO filler fraction, reaching up to 3.2 ± 0.5 and 109.3 ± 12.7 GPa, respectively, with a drawing ratio of 60× and a very low TrGO weight fraction of 1%. These values represent by far the highest reported to date for a polymer/graphene composite. Experimental characterizations indicate that as the polymer films are drawn, TrGO fillers are exfoliated, which is further confirmed by molecular dynamics (MD) simulations. Exfoliation increases the specific area of the TrGO fillers in contact with the PE matrix molecules. Molecular dynamics simulations show that the PE−TrGO interaction is stronger than the PE−PE intermolecular van der Waals interaction, which enhances load transfer from PE to TrGO and leverages the ultrahigh mechanical properties of TrGO.**

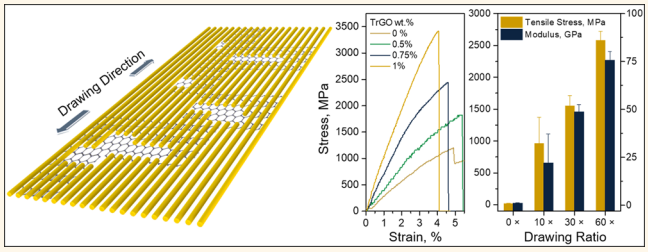


**KEYWORDS:** *graphene, polyethylene, nanocomposite, drawing ratio, mechanical strength*

Lightweight polymers with superior mechanical properties are desirable in many applications, such as structural materials, ballistic protection, and packaging.[1−3] Ultrahigh tensile strength (~1.5−4.5 GPa) has been realized in different polymer fibers, primarily by changing the molecular structure from amorphous to highly aligned crystalline fibers using spinning and drawing processes. These are exemplified by commercial products such as Dyneema, Spectra, Kevlar, and Zylon fibers (Figure 1a, data are collected from refs 2 and 4). The crystalline fibers leverage strong intramolecular covalent bonds along the polymer chains to transfer load. In contrast, amorphous fibers have defects, and load is transferred mainly by weak intermolecular van der Waals (vdW) interactions. Polymer

Received: June 22, 2018
Accepted: January 8, 2019
Published: January 11, 2019

ACS Publications © 2019 American Chemical Society



DOI: 10.1021/acsnano.8b04734
ACS Nano 2019, 13, 1097−1106

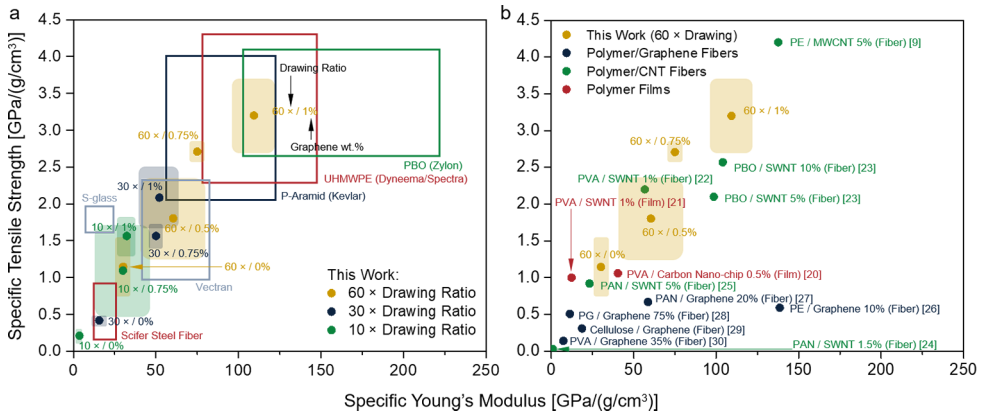


**Figure 1. Ashby charts of specific tensile strength and specific Young's modulus for the PE/TrGO films from this work compared to (a) different commercial high strength, and (b) different polymer carbon nanomaterial [e.g., single- and multiwalled carbon nanotubes (SWNT and MWCNT), graphene derivatives] composites. Note: for better comparison among different materials, specific mechanical properties, which are the measured properties divided by density, are plotted. Absolute mechanical property values are included in the SI.**

films can be fabricated in a higher mass production rate than fibers, but usually exhibit lower crystallinity and much lower mechanical properties[5,6] compared with the more confined fibers, where the chain alignment is much better (see Figure 1b). Reinforcing polymers with strong inorganic fillers, especially carbon nanotubes (CNTs), has led to significant improvement in mechanical properties[7,8] with fiber strength up to ∼4.2 GPa and Young's modulus up to 137.0 GPa.[9] Graphene has similar mechanical properties as CNTs,[10−12] and graphene composites have also attracted tremendous interest.[13−15] However, graphene fillers in composites do not enhance mechanical properties as effectively as CNT composites.[16−19] A comparison of different polymer/CNT and polymer/graphene fibers shows this disparity (Figure 1b).[9,20−30]

In this work, lightweight polyethylene/thermally reduced graphene oxide (PE/TrGO) composite films are fabricated from a roll-to-roll drawing process and shown to exhibit superior mechanical properties, up to 3.2 ± 0.5 GPa in specific tensile strength and 109.3 ± 12.7 GPa in specific Young's modulus (or 3.1 ± 0.5 GPa in absolute tensile strength and 106.0 ± 12.3 GPa in absolute Young's modulus). These values represent by far the highest properties reported for polymer/graphene composites and are comparable to the best commercially available polymer fibers (Figure 1a) and polymer/CNT composites (Figure 1b). Our results also indicate that the weight fraction of the TrGO filler and the drawing ratio can significantly impact the mechanical properties of the nanocomposite films. Experimental characterization [e.g., wide-angle X-ray diffraction (WAXD), Raman microscopy, transmission electron microscopy (TEM), scanning electron microscopy (SEM), polarized Fourier transform infrared (FTIR)] and molecular dynamics (MD) simulations indicate that the achieved mechanical properties are due to (1) highly aligned PE molecular chains from the drawing process such that axial load is largely carried by the strong intramolecular covalent bonds along the backbone, (2) exfoliation of TrGO dispersed in the polymer matrix during the drawing process such that the specific surface area is increased, and (3) PE−TrGO interactions that are stronger than the PE−PE intermolecular vdW interaction such that load is transferred from PE to TrGO and thus leverage the ultrahigh mechanical properties of TrGO.

Polymers are used in a wide range of applications due to their low density, low cost, ease of processing, nontoxicity, biocompatibility, and chemical resistance.[31] However, since polymers in the bulk amorphous phase have entangled molecular chains, voids, and other defects, they usually have very low stiffness and strength.[32] Studies have shown that aligned crystalline polymer fibers can exhibit much greater mechanical properties because the load is carried by the strong covalent bonds along the polymer chains.[33−35] Recent studies[32,36] on PE nanofibers (70−260 nm in diameter) fabricated using multistep ultradrawing reported the tensile strength can reach up to 11.4 GPa and Young's modulus of 312 GPa due to a near 100% crystallinity. However, these nanofibers have a low production rate, and the small fiber diameters pose challenges for their practical applications.

Polymer films are more amenable to large-scale production than fibers, and thus promise to expand applications of polymers and make existing applications more advantageous and cost-effective. To improve the mechanical performance of neat polymer films, strategies like zone annealing and melt/drawing have been implemented.[37,38] However, the drawing ratio cannot reach the same level as polymer fibers. The crystallinity of these films is usually <40%, and the mechanical properties are much lower than those of most high strength fibers.[39] Loomis et al.[40] recently developed a process of combining chain disentanglement extrusion and hot-drawing to achieve very high crystallinity PE films (>99%), which has enabled ultrahigh thermal conductivity of 62 W/mK.[41] This process may also provide an ideal platform for producing high strength neat PE films.

The addition of nanoscale reinforcements in polymers is also a well-known method to significantly enhance mechanical properties. CNTs have been the primary nanoscale reinforcement investigated over the past two decades. Polymer/CNT composite films indeed exhibit high strength (∼1.0 GPa in specific tensile strength, Figure 1b).[20,21] Graphene and its derivatives, which have been extensively explored in many fields, such as electrochemical energy storage,[42] water purification,[43,44] and as a media to improve the utilization of other materials,[45] have gained interest as nanoscale polymer reinforcement in recent years due to similar intrinsic mechanical properties[46] to CNTs with easier mass production.[13,47−50] However, polymer/graphene composite fibers have not lived up to their expectations, with inferior mechanical properties compared with polymer/CNT composites (Figure 1b). A high strength



DOI: 10.1021/acsnano.8b04734
ACS Nano 2019, 13, 1097−1106

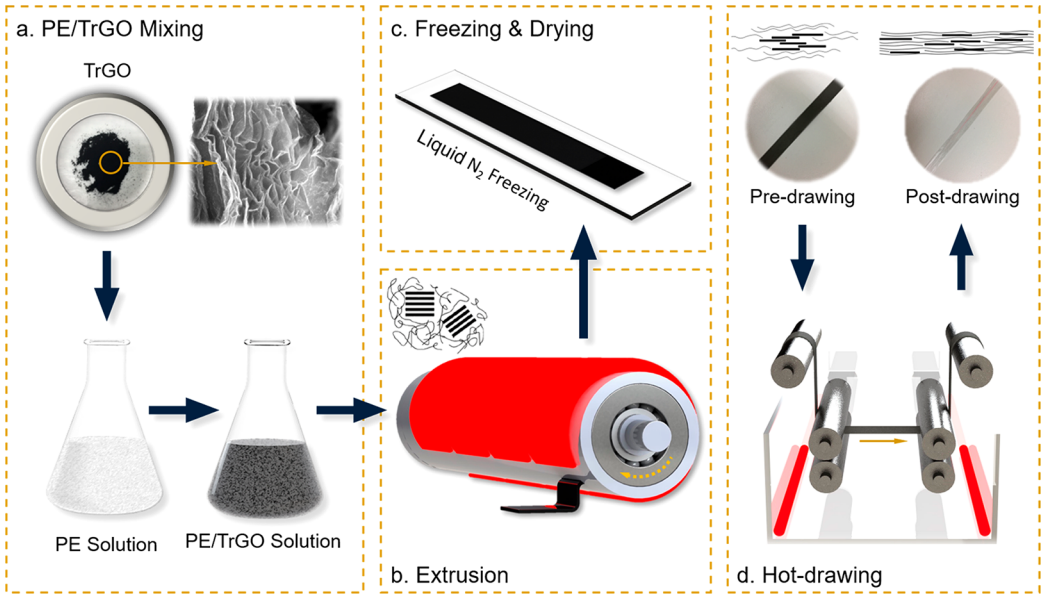


**Figure 2. Schematic diagram of the PE/TrGO film fabrication process involving (a) PE/TrGO mixture solution preparation, (b) high shear rate extrusion for chain disentanglement and TrGO exfoliation, (c) low temperature freezing and drying of the microstructure in the gel, and (d) mechanical hot-drawing to form the eventual PE/TrGO nanocomposite film.**

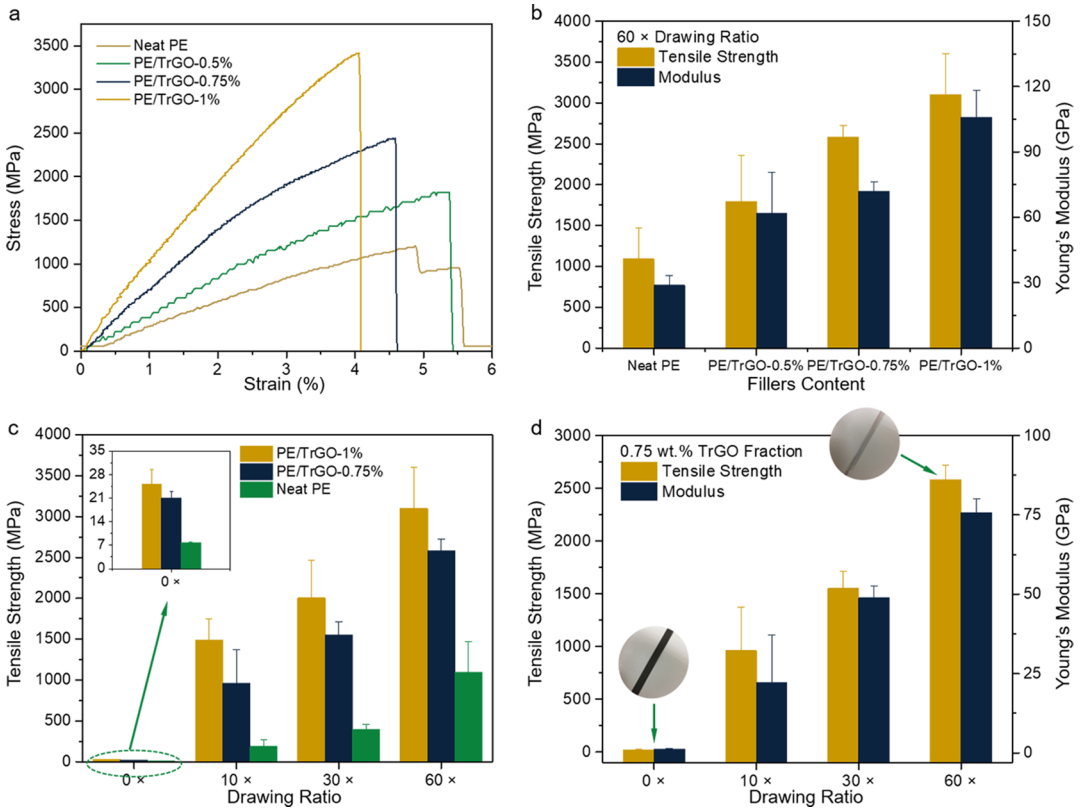


**Figure 3. (a) Typical strain−stress curves of PE/TrGO composite films with 60× drawing ratios and different filler fractions. (b) Tensile strength and Young's modulus of neat and composite films (60× drawing ratio) with different filler fractions. (c) Tensile strength of neat and composite films (0.75% and 1% filler fraction) with different drawing ratios. (d) Tensile strength and Young's modulus of composite films (0.75% filler fraction) with different drawing ratios. (b−d) Error bars show one standard deviation of mean measurement for each group.**

polymer/graphene composite film has not been previously reported to our knowledge.

Therefore, in this study, we integrate nanoscale reinforcements into the extrusion-drawing process[40] to fabricate PE/TrGO composite films with superior mechanical properties. Briefly, TrGO powder (see the Supporting Information (SI) for TrGO characterization) is added to a PE/decalin solution (Figure 2a), which is then extruded at a high shear rate to disentangle the polymer chains and exfoliate the TrGO (Figure 2b). The extruded composite solution is then frozen at low



DOI: 10.1021/acsnano.8b04734
ACS Nano 2019, 13, 1097−1106

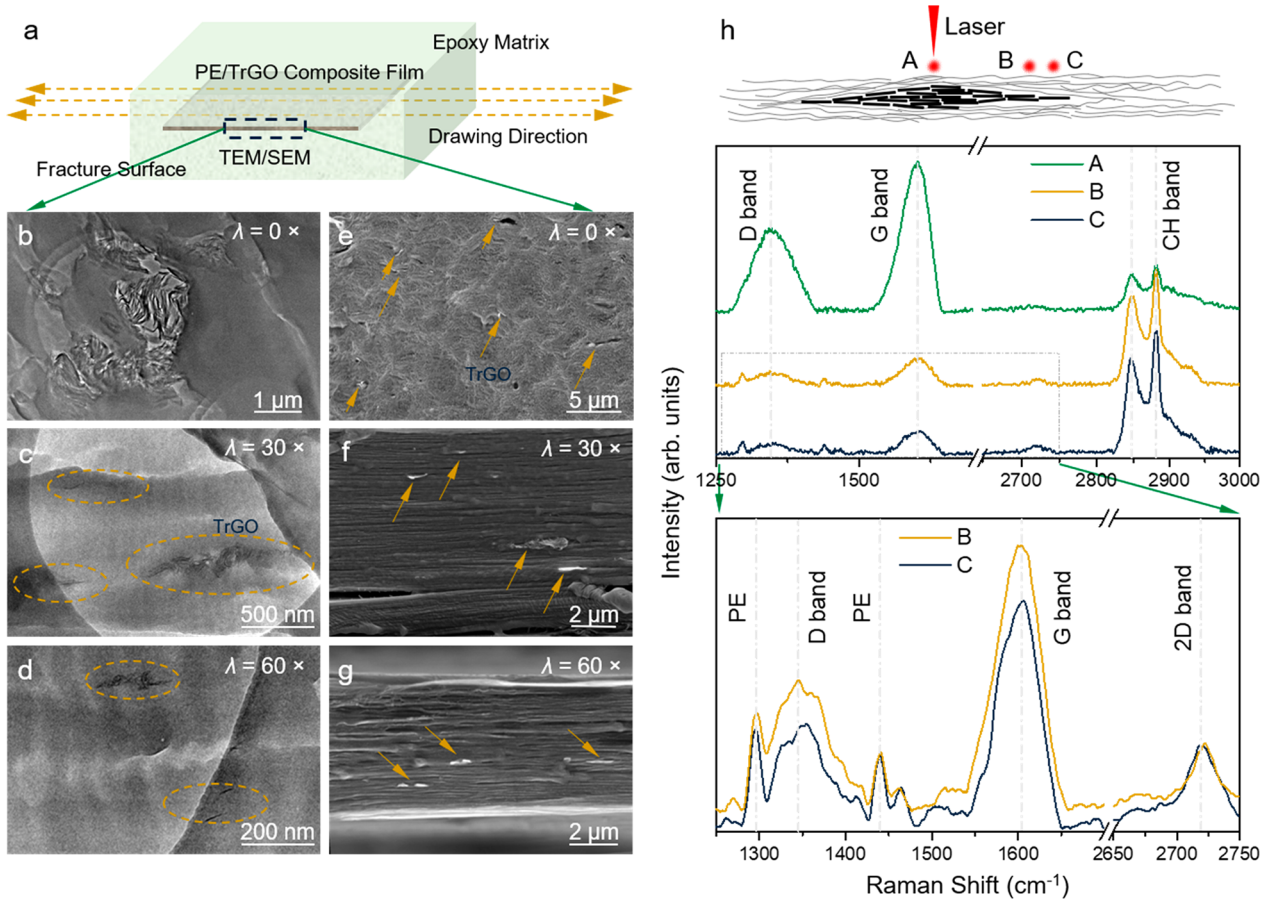


**Figure 4. (a) Schematic of the cross-sections exposed for the TEM and SEM images of samples with 1 wt % TrGO. (b–d) TEM images of TrGO fillers within the PE matrix at different drawing ratios (λ). As the film is drawn, the filler clusters obviously align along the drawing direction. As the drawing ratio increases, the sizes of TrGO filler clusters also appear to be smaller, which may suggest that TrGO clusters are gradually separated. (e–g) SEM images of TrGO fillers within the PE matrix at different drawing ratios (λ). The drawn films display better aligned filler clusters along the drawing direction. (h) Top: schematic of drawing-induced exfoliation of TrGO fillers and the location of micro-Raman detection spots. Bottom: the Raman shifts measured at each of the three detection spots reveal that the number of graphene layers becomes progressively smaller as the spot approaches the edge of the cluster, consistent with the exfoliation mechanism illustrated in the schematic.**

temperature and dried to obtain a solid film (Figure 2c). This film is then drawn at elevated temperature to form the final composite films (Figure 2d). The high internal shear stress in the drawing process also helps further exfoliate the TrGO. Different drawing ratios (10×, 30×, and 60×) and TrGO weight fractions (0.5%, 0.75%, and 1%) are investigated. Note that higher concentrations of TrGO were attempted, but the high viscosity prevented successful extrusion of the solution. As-prepared samples are then characterized using the optical microscope, WAXD, Raman spectroscopy, TEM, SEM, and polarized FTIR. The mechanical properties of films are measured in uniaxial tension. Details of the composite film fabrication, material characterization, and mechanical testing are included in the Experimental Section.

## RESULTS AND DISCUSSION

Representative strain–stress curves of the PE/TrGO composite films with 60× drawing ratios and different filler fractions are shown in Figure 3a. The tensile strength and Young's modulus increase with an increase in TrGO fraction (Figure 3b), as expected due to the higher intrinsic strength and stiffness of TrGO compared with the PE matrix. This trend is consistent with previous measurements for other PE/CNT and PE/graphene fiber composites.[21,23−25] Interestingly, even at very low TrGO filler fractions (<1%), the mechanical property enhancements are significant. For example, with only 1 wt % of TrGO, the tensile strength of the PE film with 60× drawing ratios is increased from 1.1 to 3.1 GPa—a 182% enhancement, and meanwhile, the modulus is increased by more than 3-fold (in the following text, we use absolute strength and modulus instead of specific ones since comparisons are made among the same PE composites). Such significant improvements in mechanical properties with low filler fractions have also been observed previously in bulk polymer/graphene composites[48] and polymer/CNT composite fibers,[22,24] which were largely attributed to the good dispersion of the fillers and their very high specific surface areas that help distribute load from the polymer matrix to the strong fillers.[51]

We further note that the level of mechanical property enhancement is more significant than those achieved in high strength polymer/CNT composite fibers (e.g., enhancement is less than 100% with up to 5 wt % CNT),[9,22,23] which may be attributed to the fact that graphene, as a 2D sheet, has a larger specific surface area than CNTs.[48,51] In general, the specific area of the TrGO fillers is further increased when they are fully exfoliated. In our film preparation process, there are two steps that progressively enhance the exfoliation, including the high shear rate extrusion and mechanical drawing. Previous experi-



DOI: 10.1021/acsnano.8b04734
ACS Nano 2019, 13, 1097−1106

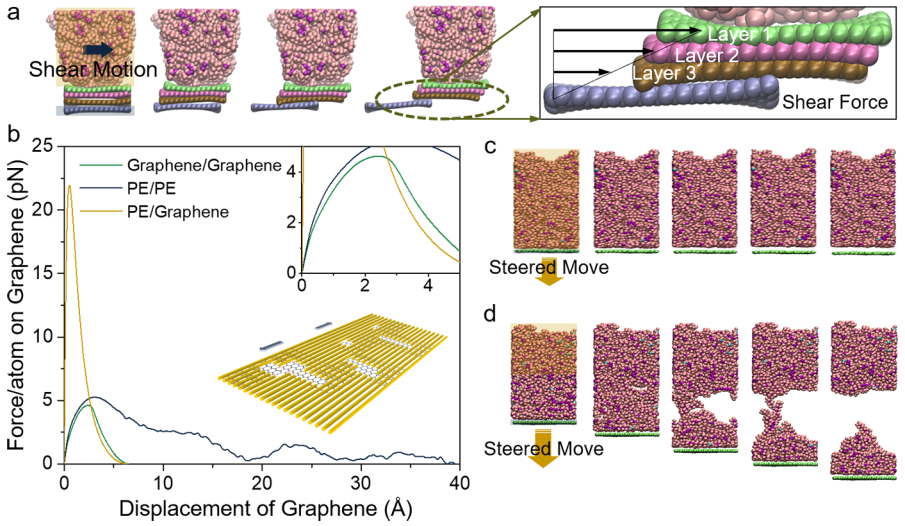


**Figure 5. (a) MD simulation of a PE/multiple layer graphene junction, where the bottom graphene layer is fixed, and PE is sheared using steered MD. The snapshot shows the relative displacement increase of graphene layers indicating that the shearing PE can lead to exfoliation of graphene stacks. (b) Force as a function of displacement of graphene obtained from the steered MD simulations shown in parts c and d. As a comparison, the force to pull two graphene layers apart is also shown. The inset schematic shows exfoliated graphene overlaps with a large number of aligned PE chains to effectively transfer load from the PE matrix to the graphene filler. (c) A graphene layer is pulled away from the contacting PE junction by steered MD with the whole PE part fixed. (d) A graphene layer is pulled away from the contacting PE junction by steered MD with the top half of the PE fixed.**

ments have shown that drawing is very effective in exfoliating layered fillers embedded in polymer matrices.[20,52] In a previous study, hexagonal-BN (*h*-BN) filler was found to be exfoliated into even single layers when a PE/*h*-BN composite fiber is drawn.[52] It is known that the interlayer interaction between *h*-BN layers is stronger than that between graphite layers.[53,54] Thus, the exfoliation of TrGO should have happened more easily in our drawing process. Additionally, the TrGO particles are already partially exfoliated during the first few material preparation steps (sonication and extrusion). When the composite films are drawn, the different layers in an aggregated TrGO cluster move with the adjacent polymer chains, expanding the spatial extent of the cluster (Figure 2d). This process increases the specific surface area of the fillers so that there is more contact with the surrounding polymer chains.

The conformation of TrGO fillers during the drawing process is characterized by cross-sectional TEM, SEM (see Figure 4a for the imaging cross-section), and Raman spectroscopy on selected samples. TEM images (Figure 4b–d) show the conformation of TrGO fillers within the PE matrix. When the composite film is not drawn (Figure 4b), the TrGO fillers are aggregated and randomly oriented. As the drawing ratio increases, filler clusters expand such that TrGO flakes align along the drawing direction. There is also the decrease in the size of clusters, which suggests that the TrGO flakes are being exfoliated (Figure 4c,d). SEM images (Figure 4e–g) show TrGO fillers within the film samples with three different drawing ratios. As the film is drawn, the TrGO fillers become aligned with the drawing direction. We should note that since the filler distributions are random, and the cross-sections are also exposed at random locations, it is impossible to monitor the conformation change of the same filler cluster. While the above observations are only qualitative, the general trend that the fillers become aligned along the drawing direction is valid. SEM is also employed to image the top surface of composite films (Figure S8), which also indicates that TrGO clusters become more separated. We have also used micro-Raman to probe the graphene peaks around a visually less transparent spot in a film with 30× drawing ratio and 0.75% TrGO fraction. As the Raman laser (~1 $\mu$m in diameter) moves from approximately the center of the dark spot toward the edge, with a total distance of 10 $\mu$m along the drawing direction, the intensity of the G peak decreases while that of the 2D peak increases (Figure 4h and Figure S9). Since it is known that the ratio of $I_{2D}/I_G$ is strongly correlated to the number of graphene layers,[55] according to the comparison between the $I_{2D}/I_G$ ratios at points A, B, and C, we can conclude that the number of layers in the graphene cluster is decreasing along the testing track, which may be attributed to the drawing-induced exfoliation as schematically illustrated at the top of Figure 4h.

To further confirm that the hot-drawing process can indeed lead to graphene exfoliation, we performed MD simulations to simulate the shearing phenomenon of PE in contact with a few layers of graphene. The simulation domain consists of a polymer block in contact with a stack of graphene layers with the bottom layer fixed (Figure 5a). As the polymer is collectively sheared in parallel to the graphene layers, the graphene layers displace relative to each other. These results suggest that, during the drawing process, as polymer chains are subject to relative movements inside the film, the graphene stacks can be exfoliated. These observations also suggest that the interaction between the polymer and graphene is stronger than that between graphene layers, and thus provide an atomistic level mechanism for drawing-induced exfoliation.

The theoretical strength and modulus of a perfect crystalline PE (strength >11 GPa and modulus >370 GPa)[36,56] are still much larger than the ones measured here for the PE/TrGO composite films, since the mechanical behaviors of our films are still limited by the intermolecular vdW interactions (i.e., aligned chains can still slide relative to one another when subject to strain). In this scenario, for the TrGO filler to enhance the already high mechanical property of PE films, it is important that the interactions between PE molecules and graphene are stronger than those among the PE molecules themselves. Here, we calculate the real-time forces on the graphene layer in



DOI: 10.1021/acsnano.8b04734
*ACS Nano* 2019, 13, 1097–1106

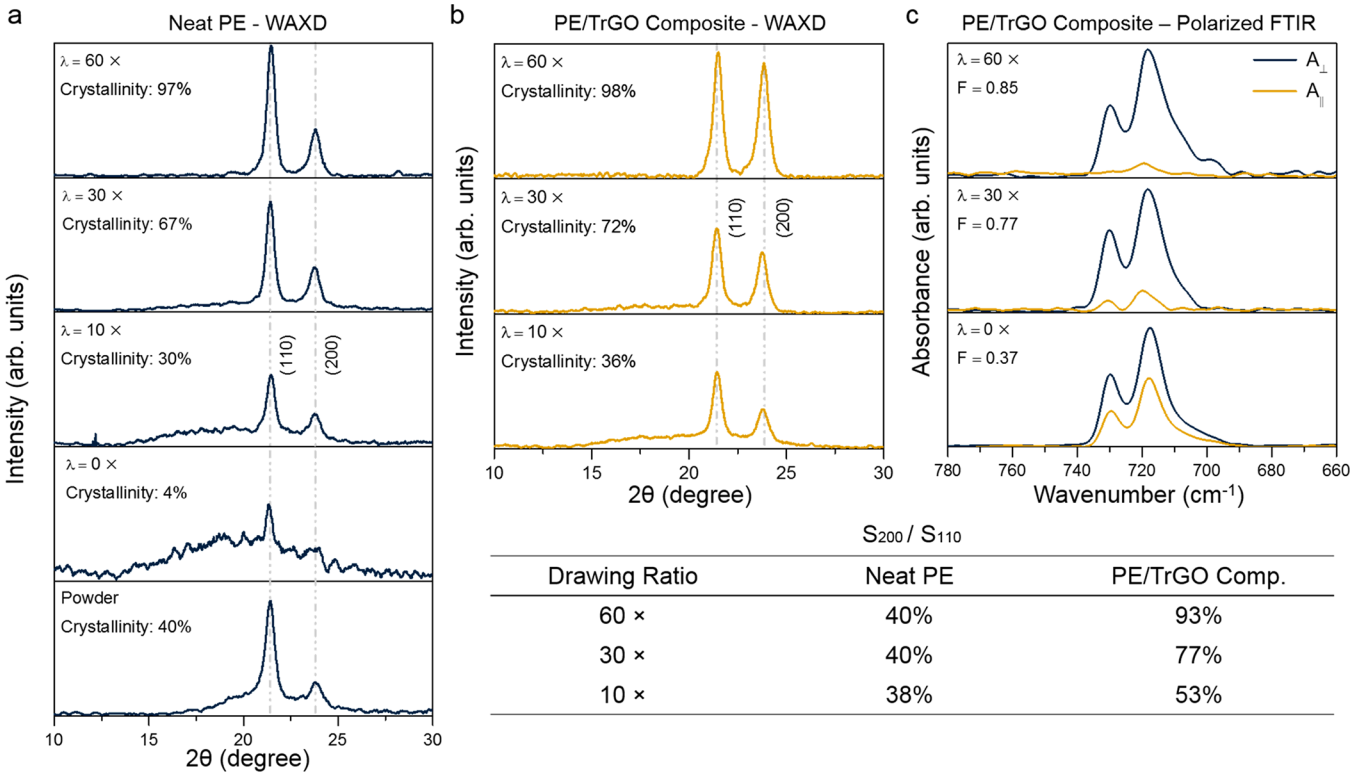


$S_{200}$ / $S_{110}$

| Drawing Ratio | Neat PE | PE/TrGO Comp. |
|---|---|---|
| 60 × | 40% | 93% |
| 30 × | 40% | 77% |
| 10 × | 38% | 53% |

**Figure 6. (a) WAXD spectra of neat PE. From top to bottom: neat PE films with 60×, 30×, 10×, and 0× drawing. The bottom-most panel shows the spectrum of the as-purchased PE powder. Inside each panel, the calculated crystallinities are shown. (b) WAXD spectra of PE/TrGO composite films with different drawing ratios. The table shows the ratio between the (200) and the (110) peaks for both neat and composite samples. (c) Polarized FTIR spectra and the calculated orientation functions ($F$) of PE/TrGO composite films with different drawing ratios.**

steered MD simulations, where we pull the graphene layer away from the polymer block. In one case, we fixed all the polymer molecules, and in another case, we fixed half of the polymer block (Figure 5c,d). In the second case, when the graphene is pulled away from the polymer, the breakage of the structure happens within the polymer block, and a few polymer chains adhered to the graphene surface (Figure 5d), suggesting that the interaction between the graphene and polymer is stronger than that within polymer. As seen from Figure 5b, the force needed to break the graphene away from the polymer (Figure 5c) is indeed much larger than that needed to break the polymer apart (Figure 5d), which is consistent with the observation in Figure 5d and a previous simulation study.[57] These results suggest that the interaction between the polymer and the contacting graphene layer is strong, and thus load transfer from the polymer matrix to the TrGO fillers will be efficient and beneficial to the overall mechanical properties. From the SEM images in Figure S8 (bright arrows), the lateral sizes of the exfoliated TrGO are estimated in the range 1−5 $\mu$m, which are much larger than the intermolecular lattice constants of the PE crystal (0.74 and 0.49 nm).[58] The size of TrGO flakes estimated from the SEM images is similar to our previous AFM measurements[59] and other reports.[60,61] This allows the dispersed TrGO fillers, especially when exfoliated, to have significant spatial overlap with a large number of PE chains (Figure 5b, inset).

This will not only replace many weaker vdW interchain interactions with relatively stronger graphene−PE interactions, but also help maximize the effect of TrGO since the load can be efficiently transferred from the matrix to the filler. In addition, according to previous studies, the extremely small thickness compared to the lateral dimensions of exfoliated TrGO can easily lead to a wrinkled topology,[62−64] which is also believed to improve the mechanical interlocking with polymer chains and thus further enhance adhesion at the PE−TrGO interface.[65] We also note that the peak forces needed to pull graphene away from polymers in both cases (i.e., Figure 5c,d) are larger than that needed to pull two graphene layers apart (see Figure 5b), which suggests that the exfoliation of graphene stacks can happen even before chain disentanglement. This implies that the extrusion process can also contribute to exfoliating the TrGO clusters in our experiments.

Another important observation is that the tensile strength and Young's modulus of both neat PE and PE/TrGO composite films increase with a higher drawing ratio (Figure 3c,d). This is directly related to the crystallinity of the drawn films, as it is well-known that higher crystallinity can lead to greater mechanical properties.[32,36,66,67] WAXD measurements (Figure 6a) confirmed that the signature PE peaks ($2\theta$ = 21.5° and 24°), corresponding to the (110) and (200) Bragg reflections of the PE crystalline structure, are enhanced significantly as the drawing ratio increases. The crystallinities of the neat films with 0×, 10×, 30×, and 60× drawing ratios are respectively 4%, 30%, 67%, and 97% as calculated from the percentage of crystalline PE scattering peak intensity with respect to the total scattering intensity (see the SI for more details).[68] This result indicates that, as the drawing ratio increases, the film is gradually transformed from the amorphous to the crystalline phase. It is worth noting that, for the as-extruded polymer film (i.e., 0× drawing ratio), the peaks are very weak, and the crystallinity is much lower than the PE powder (40%, Figure 6a) which has dispersed lamellar structures. This suggests that the high shear extrusion is effective in disentangling the PE chains. The as-



DOI: 10.1021/acsnano.8b04734
ACS Nano 2019, 13, 1097−1106

extruded film also exhibits lower mechanical properties than nonextruded, nondrawn PE films (Table S3 in the Supporting Information).

WAXD measurements are also performed on the PE/TrGO composite films with 0.75% filler fraction and various drawing ratios (Figure 6b). Like the neat films, the intensities of both PE peaks increase as drawing ratio increases. The overall crystallinities of the composite films are also slightly increased compared to those of the neat films with the same drawing ratios, which agree well with previous studies showing enhanced crystallization of PE with the presence of graphene fillers.[22,69−71] We note that TrGO should also have a WAXD peak around 24°, overlapping with the PE (200) peak. However, since the TrGO fraction is small (0.75%), we do not expect that its existence has contributed significantly to the overall peak intensity used to calculate the PE crystallinity.

Polarized FTIR testing can help us learn that such high crystallinities are strongly related to the fact that the orientations of polymer chains gradually become uniform during the drawing processing, and similar findings have also been discussed in other studies.[72−74] In our work, the orientation functions, which are used to evaluate the orientation characteristic of the polymer chains, of the composite films (0.75 wt %) with 0×, 30×, and 60× drawing ratios can be estimated, respectively, to be 0.37, 0.77, and 0.85 according to the intensity ratios between the shown $A_{\parallel}$ and $A_{\perp}$ around the peaks of 720 and 730 $cm^{-1}$ in Figure 6c (see the SI for the details of the calculation method). Thus, the drawing process can be proven once again to have a positive influence on the mechanical properties for the composite films by aligning the polymer chains.

Another important observation is on the ratios of the two PE peaks ($S_{200}/S_{110}$) in the WAXD spectra, which stay almost unchanged for the neat PE films when drawn but increase significantly when the PE/TrGO composite films are drawn (Figure 6, table). It is likely that the PE order in the (200) plane is related to the preferential crystallization orientation at the vicinity of the TrGO fillers. As the drawing ratio increases, more TrGO surfaces become available for PE preferential crystallization, and thus the PE (200) peak intensity increases. This observation provides additional proof for the drawing-induced filler exfoliation as it can provide larger specific surface areas for PE crystallization. Moreover, the dramatically increased PE (200) peak has also been claimed to result in further mechanical enhancement within the polymer phase.[75] Thus, for the drawn composite films, the property improvements may be a combination of the filler enhancement from the TrGO fillers and the enhancement within the PE matrix itself. If we use a simple mixing rule ($E_c = fE_f + (1 - f)E_m$, where $f$ is the volume fraction of the filler, $E_f$ is the property of the filler, and $E_m$ is the property of the matrix) to express the composite properties, we can back out the PE matrix strength and modulus to be ∼2.55 and ∼101.7 GPa, respectively, for the 60× drawing ratio. These are much improved over the neat PE films with the same drawing ratio but are lower than recently measured ultrahigh crystalline PE fibers (strength, 11.4 GPa; and modulus, 312 GPa).[32,36]

## CONCLUSIONS

In summary, we have demonstrated ultrahigh mechanical properties in PE/TrGO nanocomposite films fabricated from high shear rate extrusion and mechanical drawing. The highest average tensile strength and Young's modulus achieved are 3.1 ± 0.5 and 106.0 ± 12.3 GPa, respectively, which are comparable to some of the best high strength polymer fibers known (Figure 1a). These also represent by far the highest values reported for any polymer/graphene composite (Figure 1b). Such an enhancement is partially from the effect of PE crystallization after drawing. In addition, the high shear rate extrusion and mechanical drawing also help exfoliate the TrGO fillers in the PE matrix, which significantly increases the specific area of the fillers. Due to the strong PE−graphene interaction, mechanical load can efficiently transfer from the polymer matrix to the fillers, taking full advantage of the superior intrinsic strength of graphene (TrGO). These results provide useful insights for understanding the mechanism of strength improvement in PE/TrGO composites and offer guidance for further improvement. The same strategy may be transferable to design other, new high strength polymer composite materials. Due to the advantage of the larger dimension compared to fibers, the nanocomposite films of this study can potentially substitute for fiber-reinforced polymers in applications requiring lightweight structural materials.

## EXPERIMENTAL SECTION

**Material Synthesis.** A four-step process is implemented to produce nanocomposite films, including (1) PE/TGO mixing, (2) high shear rate sol−gel extrusion, (3) structural freezing and drying, and (4) mechanical drawing. The extrusion and film drawing process are performed on a continuous fabrication system similar to the one employed by Loomis et al.[40] The schematics of the procedures are shown in Figure 2.

TrGO powder is prepared using the methods previously reported by Yang et al.[59] Thermal reduction helps significantly reduce the oxygen groups (see the SI for XPS characterization),[63,64,76] which increases the mechanical properties, and also helps expand the graphene layers,[59,77] which is beneficial for further exfoliation during drawing. The TrGO flakes are measured to be as thin as ∼0.6 nm.[59] To prepare the PE/TrGO mixture solution (Figure 2a), ultrahigh molecular weight PE powder of 3−6 × $10^6$ g/mol is added to the decahydronaphthalene solvent (both from Sigma-Aldrich) to form a dilute solution with 3 wt % PE. Different amounts of TrGO powder are added to the PE solution to achieve different weight fractions (0%, 0.5%, 0.75%, and 1%) in the final composite. To facilitate TrGO dispersion in the solution, ultrasonic stirring is performed for 30 min. The solution is then uniformly heated to 150 °C in an oil bath and maintained at this temperature for 24 h. Antioxidant (2,6-di-*tert*-butyl-4-methyl-phenol, Sigma-Aldrich) with a concentration of 0.5 wt % to PE is added to prevent oxidation during the dissolution process. The mixture is magnetically stirred for 24 h to ensure complete dissolution.

The PE/TrGO solution is then fed into an extrusion machine (Figure 2b), where the whole flow channel is heated and maintained at 120 °C. The solution is pressed through the extrusion chamber by pressurized air with a constant pressure of 140 kPa. A solid cylinder inside the cylindrical extrusion chamber is driven by a DC motor at a speed of 1900 rpm to generate a Couette flow to initiate a uniform high shear rate to the PE/TrGO solution when it passes through a 1 mm gap between the two cylinder surfaces. The high shear rate can significantly disentangle the PE polymer chains[40] and help further disperse and exfoliate the TrGO. The extruded solution exits the chamber onto a liquid $N_2$-cooled substrate to freeze the internal microstructure (Figure 2c). The solvent is then evaporated at ambient conditions over 24 h, forming a stable film.

The dried film is then fed into a mechanical drawing system which is heated and maintained at 85 °C to soften the film and ensure drawability (Figure 2d). Different drawing ratios (10×, 30×, and 60×) are applied. The disentangled polymer chains become increasingly aligned and crystallized as the drawing ratio increases. Because of the high internal strain during the drawing process, further TrGO exfoliation is also achieved.

**Characterization Methods.** TrGO fillers within the PE matrix are imaged by TEM (FEI Tecnai F30) (Figure 4b−d) and SEM (EVO 50



DOI: 10.1021/acsnano.8b04734
ACS Nano 2019, 13, 1097−1106

LEO, Carl Zeiss) (Figure 4e–g) using the sample preparation methods provided in the SI. The morphology of TrGO fillers (Figure S2) and the dimensions of the composite films (e.g., Figure S3a) are also characterized by SEM. A typical plot of the thickness reduction as a function of drawing ratio is included in Figure S4. WAXD (Bruker D8 Advance Davinci) is performed at room temperature using Cu K$\alpha$ radiation ($\lambda$ = 1.5418 Å) over 9–60° 2$\theta$ using a step size of 12° and a step time of 0.5 s. Detailed WAXD analysis data are included in Table S2 of the Supporting Information. The orientation of polymer chains for the drawn composite film is monitored by polarized FTIR (Nicolet 6700 spectrometer). At each drawing ratio, polarized infrared spectra (by rotating a ZnSe polarizer), parallel and perpendicular to the drawing direction, respectively, are collected with a resolution of 2 $cm^{-1}$ in reflection mode. Micro-Raman spectroscopy (NRS-5100, Jasco) is employed to characterize the structure of the TrGO filler in the PE matrix. A Nikon Eclipse Ti–E inverted optical microscope is used to observe the film surface optically (Figure S5).

Tensile tests are conducted under ambient conditions using an electromechanical load frame (Bose Electro Force 3300). The drawn film is split into narrow ribbons which are mounted with a 14 mm gauge length for testing using methods described elsewhere.[78] Polymer film ribbons are loaded at a crosshead speed of 0.1 mm/s until failure (Figure S3c). Young's modulus and the ultimate tensile strength are calculated from the measured force–displacement data, gauge length, and cross-sectional area of ribbons. Measurements are reported as the mean (±standard deviation) of replicates ($n$ = 3–10 specimens/group). Load and displacement data were collected at 10 Hz using a 5 lb load cell (MBP-5, Interface) and linear variable displacement transducer (LVDT), respectively. Apparent stress and strain were calculated based upon the dimensions of the rehydrated scaffolds measured prior to loading using digital calipers (±0.01 mm). The zero strain point was set at first region of the stress–strain curve exhibiting a slope of 5 kPa or higher within a 2% strain range. The scaffold compressive modulus was measured as the maximum slope of the stress–strain curve over a 5% strain range within 0–20% strain.

**MD Simulations.** All MD simulations are performed using the large-scale atomic/molecular massively parallel simulator (LAMMPS). The Tersoff potential, which has been shown to predict reasonable values for the thermomechanical properties of graphene,[79,80] is used to describe the graphene interactions in this work. For PE, the polymer consistent force field (PCFF) potential[81] is employed, since the PCFF potential is widely used to study the physical properties of polymers.[82] The interactions between graphene and PE are vdW interactions, which are modeled by Lennard–Jones (L–J) potentials.[83] Lorentz–Berthelot mixing rules are used to obtain the L–J parameters across different species of atoms. The L–J parameters of different atoms used in this study are listed in the SI, Table S1. An L–J force cutoff of 10 Å is used. The amorphous PE ($C_{60}H_{122}$) is constructed using the Material Studio software in this study. After several iterations of annealing (heating and slow cooling) processes, which are used to release any stress inside the PE block, the density is found to be 0.90 g/$cm^3$ at 300 K and 1 atm, which matches experimental data of 0.88–0.96 g/$cm^3$.[84]

For the PE/graphene interface simulation, graphene layers are placed beneath the PE block to form interfaces (Figure 5a,c,d). Five different cases (Figure S6) are studied to simulate the exfoliation process and calculate different interactions (polymer–graphene, polymer–polymer, and graphene–graphene). For the simulation of the graphene layer exfoliation, the simulation domain size is 30 Å × 30 Å × 50 Å. A periodic boundary condition is used along the $y$-direction, and the amorphous polymer is built with the same periodicity as the graphene layers. Free boundary condition is used in the $x$-direction to visualize sheering in this direction. Also, a periodic boundary condition is used in the $z$-direction, and a vacuum is left above the polymer top to avoid interactions between the polymer and the periodic image of graphene. However, before the production run, the polymer structure is optimized at 300 K with periodic boundary conditions applied to both the $x$- and $y$-directions and a constant volume. After optimization, the polymer block is then sheared collectively with respect to the graphene layers, during which the bottom layer graphene is fixed. To calculate the three types of interactions, simulation cells with the dimension of 30 Å × 30 Å × 100 Å are constructed (e.g., Figure 5c,d). Periodic boundary conditions are used along three directions, while a vacuum space is intentionally reserved at the top and bottom along the pulling direction. The graphene layer is pulled away from the polymer block in the direction perpendicular to the graphene. The separation is realized by displacing the graphene at a constant speed. The $z$-component (perpendicular to graphene) of the total force acting on the moving graphene layer is recorded and plotted in Figure 5b. Depending on the force of interest, different parts of the simulation cells (e.g., polymer, graphene, or half of polymer) are fixed during the pulling simulations as indicated in the corresponding figures. Figure S6 summarize all simulated molecule structures.

## ASSOCIATED CONTENT

### Supporting Information

The Supporting Information is available free of charge on the ACS Publications website at DOI: 10.1021/acsnano.8b04734.

Raman microscopy characterization method, calculations of crystallinity and molecular orientation function, TEM/SEM sample preparation, XPS analysis of TrGO fillers, and additional figures (PDF)

## AUTHOR INFORMATION


### Corresponding Author

*E-mail: tluo@nd.edu.

### ORCID

Yunsong Pang: 0000-0003-0522-4292
Dezhao Huang: 0000-0002-1413-5438
Fan Lei: 0000-0002-5428-9087
Eungkyu Lee: 0000-0002-0211-0727
Yajiang Huang: 0000-0002-1803-1580
Ruilan Guo: 0000-0002-3373-2588
Tengfei Luo: 0000-0003-3940-8786

### Author Contributions

¶Y.P. and J.Y. contributed equally to this work.


### Notes

The authors declare no competing financial interest.

## ACKNOWLEDGMENTS


The characterization was carried out in the Notre Dame Materials Characterization Facility and the Integrated Imaging Facility. The computation work was performed at the Notre Dame Center for Research Computing. Y.P. thanks Zhi Guo for his help in analyzing the XRD data. Y.P. also thanks Tatyana Orlova for her assistance with SEM characterization. J.Y. and F.L. are thankful for the support from the Foundation of Shenzhen Science and Technology Innovation Committee (Grant JCYJ20170817110440310). S.P. and P.S. are supported by the US Department of Energy Office of Science, Office of Basic Energy Sciences under Award DE-FC02-04ER15533 (NDRL 5222) and thank Soumya Banerjee and Amal Sebastian for their assistance with XPS characterization. T.L. would also like to thank the Dorini Family for the endowed professorship.


## REFERENCES


(1) Chang, H.; Luo, J.; Gulgunje, P. V.; Kumar, S. Structural and Functional Fibers. *Annu. Rev. Mater. Res.* **2017**, *47*, 331–359.

(2) Yao, J.; Bastiaansen, C. W. M.; Peijs, T. High Strength and High Modulus Electrospun Nanofibers. *Fibers* **2014**, *2*, 158–186.

(3) Park, J. H.; Rutledge, G. C. 50th Anniversary Perspective: Advanced Polymer Fibers: High Performance and Ultrafine. *Macromolecules* **2017**, *50*, 5627–5642.




DOI: 10.1021/acsnano.8b04734
*ACS Nano* 2019, 13, 1097–1106

(4) Koziol, K.; Vilatela, J.; Moisala, A.; Motta, M.; Cunniff, P.; Sennett, M.; Windle, A. High-Performance Carbon Nanotube Fiber. *Science* **2007**, *318*, 1892−1895.
(5) Khatua, S. C.; Maiti, S. High Performance Polymer Films 4. Mechanical Behavior. *Eur. Polym. J.* **2002**, *38*, 537−543.
(6) Zhang, X.; Liu, T.; Sreekumar, T. V.; Kumar, S.; Moore, V. C.; Hauge, R. H.; Smalley, R. E. Poly (Vinyl alcohol)/SWNT Composite Film. *Nano Lett.* **2003**, *3*, 1285−1288.
(7) Liu, Y.; Kumar, S. Polymer/carbon Nanotube Nano Composite Fibers−a Review. *ACS Appl. Mater. Interfaces* **2014**, *6*, 6069−6087.
(8) Andrews, R.; Weisenberger, M. C. Carbon Nanotube Polymer Composites. *Curr. Opin. Solid State Mater. Sci.* **2004**, *8*, 31−37.
(9) Ruan, S.; Gao, P.; Yu, T. X. Ultra-Strong Gel-Spun UHMWPE Fibers Reinforced Using Multiwalled Carbon Nanotubes. *Polymer* **2006**, *47*, 1604−1611.
(10) Service, R. F. Materials Science. Carbon Sheets an Atom Thick Give Rise to Graphene Dreams. *Science* **2009**, *324*, 875.
(11) Yu, M.-F.; Lourie, O.; Dyer, M. J.; Moloni, K.; Kelly, T. F.; Ruoff, R. S. Strength and Breaking Mechanism of Multiwalled Carbon Nanotubes under Tensile Load. *Science* **2000**, *287*, 637−640.
(12) Belytschko, T.; Xiao, S. P.; Schatz, G. C.; Ruoff, R. S. Atomistic Simulations of Nanotube Fracture. *Phys. Rev. B: Condens. Matter Mater. Phys.* **2002**, *65*, 235430.
(13) Kuilla, T.; Bhadra, S.; Yao, D. H.; Kim, N. H.; Bose, S.; Lee, J. H. Recent Advances in Graphene Based Polymer Composites. *Prog. Polym. Sci.* **2010**, *35*, 1350−1375.
(14) Zhu, Y.; Murali, S.; Cai, W.; Li, X.; Suk, J. W.; Potts, J. R.; Ruoff, R. S. Graphene and Graphene Oxide: Synthesis, Properties, and Applications. *Adv. Mater.* **2010**, *22*, 3906−3924.
(15) Zhu, Y.; James, D. K.; Tour, J. M. New Routes to Graphene, Graphene Oxide and Their Related Applications. *Adv. Mater.* **2012**, *24*, 4924−4955.
(16) Ji, X.; Xu, Y.; Zhang, W.; Cui, L.; Liu, J. Review of Functionalization, Structure and Properties of Graphene/polymer Composite Fibers. *Composites, Part A* **2016**, *87*, 29−45.
(17) Jalili, R.; Aboutalebi, S. H.; Esrafilzadeh, D.; Shepherd, R. L.; Chen, J.; Aminorroaya-Yamini, S.; Konstantinov, K.; Minett, A. I.; Razal, J. M.; Wallace, G. G. Scalable One-step Wet-spinning of Graphene Fibers and Yarns from Liquid Crystalline Dispersions of Graphene Oxide: Towards Multifunctional Textiles. *Adv. Funct. Mater.* **2013**, *23*, 5345−5354.
(18) Jiang, Z.; Li, Q.; Chen, M.; Li, J.; Li, J.; Huang, Y.; Besenbacher, F.; Dong, M. Mechanical Reinforcement Fibers Produced by Gel-Spinning of Poly-Acrylic Acid (PAA) and Graphene Oxide (GO) Composites. *Nanoscale* **2013**, *5*, 6265−6269.
(19) Hu, K.; Kulkarni, D. D.; Choi, I.; Tsukruk, V. V. Graphene-Polymer Nanocomposites for Structural and Functional Applications. *Prog. Polym. Sci.* **2014**, *39*, 1934−1972.
(20) Song, K.; Zhang, Y.; Meng, J.; Minus, M. L. Lubrication of Poly (Vinyl Alcohol) Chain Orientation by Carbon Nano-chips in Composite Tapes. *J. Appl. Polym. Sci.* **2013**, *127*, 2977−2982.
(21) Wang, Z.; Ciselli, P.; Peijs, T. The Extraordinary Reinforcing Efficiency of Single-Walled Carbon Nanotubes in Oriented Poly (Vinyl Alcohol) Tapes. *Nanotechnology* **2007**, *18*, 455709.
(22) Minus, M. L.; Chae, H. G.; Kumar, S. Interfacial Crystallization in Gel-spun Poly (Vinyl Alcohol)/single-wall Carbon Nanotube Composite Fibers. *Macromol. Chem. Phys.* **2009**, *210*, 1799−1808.
(23) Kumar, S.; Dang, T. D.; Arnold, F. E.; Bhattacharyya, A. R.; Min, B. G.; Zhang, X.; Vaia, R. A.; Park, C.; Adams, W. W.; Hauge, R. H. Synthesis, Structure, and Properties of PBO/SWNT Composites&. *Macromolecules* **2002**, *35*, 9039−9043.
(24) Gao, J.; Itkis, M. E.; Yu, A.; Bekyarova, E.; Zhao, B.; Haddon, R. C. Continuous Spinning of a Single-Walled Carbon Nanotube− Nylon Composite Fiber. *J. Am. Chem. Soc.* **2005**, *127*, 3847−3854.
(25) Chae, H. G.; Minus, M. L.; Kumar, S. Oriented and Exfoliated Single Wall Carbon Nanotubes in Polyacrylonitrile. *Polymer* **2006**, *47*, 3494−3504.
(26) Hu, W.; Zhan, J.; Wang, X.; Hong, N.; Wang, B.; Song, L.; Stec, A. A.; Hull, T. R.; Wang, J.; Hu, Y. Effect of Functionalized Graphene Oxide with Hyper-Branched Flame Retardant on Flammability and Thermal Stability of Cross-Linked Polyethylene. *Ind. Eng. Chem. Res.* **2014**, *53*, 3073−3083.
(27) Kim, H.; Jalili, R.; Spinks, G. M.; Wallace, G. G.; Kim, S. J. High-Strength Graphene and Polyacrylonitrile Composite Fiber Enhanced by Surface Coating with Polydopamine. *Compos. Sci. Technol.* **2017**, *149*, 280−285.
(28) Hu, X.; Xu, Z.; Liu, Z.; Gao, C. Liquid Crystal Self-Templating Approach to Ultrastrong and Tough Biomimic Composites. *Sci. Rep.* **2013**, *3*, 2374.
(29) Li, Y.; Zhu, H.; Zhu, S.; Wan, J.; Liu, Z.; Vaaland, O.; Lacey, S.; Fang, Z.; Dai, H.; Li, T. Hybridizing Wood Cellulose and Graphene Oxide toward High-Performance Fibers. *NPG Asia Mater.* **2015**, *7*, No. e150.
(30) Kou, L.; Gao, C. Bioinspired Design and Macroscopic Assembly of Poly (Vinyl Alcohol)-Coated Graphene into Kilometers-Long Fibers. *Nanoscale* **2013**, *5*, 4370−4378.
(31) Mittal, V.; Luckachan, G. E.; Matsko, N. B. PE/Chlorinated-PE Blends and PE/Chlorinated- PE/Graphene Oxide Nanocomposites: Morphology, Phase Miscibility, and Interfacial Interactions. *Macromol. Chem. Phys.* **2014**, *215*, 255−268.
(32) Li, P.; Hu, L.; McGaughey, A. J. H.; Shen, S. Crystalline Polyethylene Nanofibers with the Theoretical Limit of Young's Modulus. *Adv. Mater.* **2014**, *26*, 1065−1070.
(33) Feng, W.; Bai, X. D.; Lian, Y. Q.; Liang, J.; Wang, X. G.; Yoshino, K. Well-Aligned Polyaniline/Carbon-Nanotube Composite Films Grown by *in-situ* Aniline Polymerization. *Carbon* **2003**, *41*, 1551−1557.
(34) Smith, P.; Lemstra, P. J. Ultra-High Strength Polyethylene Filaments By Solution Spinning/Drawing - 3. *Polymer* **1980**, *21*, 1341−1343.
(35) O'Connor, T. C.; Robbins, M. O. Chain Ends and the Ultimate Strength of Polyethylene Fibers. *ACS Macro Lett.* **2016**, *5*, 263−267.
(36) Shrestha, R.; Li, P.; Chatterjee, B.; Zheng, T.; Wu, X.; Liu, Z.; Luo, T.; Choi, S.; Hippalgaonkar, K.; de Boer, M. P.; Shen, S. Crystalline Polymer Nanofibers with Ultra-High Strength and Thermal Conductivity. *Nat. Commun.* **2018**, *9*, 1664.
(37) Kunugi, T.; Oomori, S.; Mikami, S. Preparation of Ultra-High Modulus Polyethylene Films by the Zone-Annealing Method. *Polymer* **1988**, *29*, 814−820.
(38) Langer, L.; Billaud, D.; Issi, J. P. Thermal Conductivity of Stretched and Annealed Poly (P-Phenylene Sulfide) Films. *Solid State Commun.* **2003**, *126*, 353−357.
(39) Kunugi, T.; Hayakawa, T.; Mizushima, A. Preparation of High Modulus and High Strength PEEK Film by the Zone Drawing/annealing Method. *Polymer* **1991**, *32*, 808−813.
(40) Loomis, J.; Ghasemi, H.; Huang, X.; Thoppey, N.; Wang, J.; Tong, J. K.; Xu, Y.; Li, X.; Lin, C.-T.; Chen, G. Continuous Fabrication Platform for Highly Aligned Polymer Films. *Technology* **2014**, *2*, 189.
(41) Xu, Y.; Kraemer, D.; Song, B.; Jiang, Z.; Zhou, J.; Loomis, J.; Wang, J.; Li, M.; Ghasemi, H.; Huang, X. Nanostructured Polymer Films with Metal-like Thermal Conductivity. 2017, arXiv:1708.06416. arXiv.org e-Print archive. https://arxiv.org/abs/1708.06416.
(42) Raccichini, R.; Varzi, A.; Passerini, S.; Scrosati, B. The Role of Graphene for Electrochemical Energy Storage. *Nat. Mater.* **2015**, *14*, 271.
(43) Khan, Z. U.; Yan, T.; Shi, L.; Zhang, D. Improved Capacitive Deionization by Using 3D Intercalated Graphene Sheet−sphere Nanocomposite Architectures. *Environ. Sci.: Nano* **2018**, *5*, 980−991.
(44) Liu, P.; Yan, T.; Shi, L.; Park, H. S.; Chen, X.; Zhao, Z.; Zhang, D. Graphene-Based Materials for Capacitive Deionization. *J. Mater. Chem. A* **2017**, *5*, 13907−13943.
(45) Saravanan, P.; Selyanchyn, R.; Tanaka, H.; Fujikawa, S.; Lyth, S. M.; Sugimura, J. Ultra-Low Friction between Polymers and Graphene Oxide Multilayers in Nitrogen Atmosphere, Mediated by Stable Transfer Film Formation. *Carbon* **2017**, *122*, 395−403.
(46) Lee, C.; Wei, X.; Kysar, J. W.; Hone, J. Measurement of the Elastic Properties and Intrinsic Strength of Monolayer Graphene. *Science* **2008**, *321*, 385−388.


DOI: 10.1021/acsnano.8b04734
*ACS Nano* 2019, 13, 1097−1106

(47) Kim, H.; Kobayashi, S.; Abdurrahim, M. A.; Zhang, M. J.; Khusainova, A.; Hillmyer, M. A.; Abdala, A. A.; MacOsko, C. W. Graphene/polyethylene Nanocomposites: Effect of Polyethylene Functionalization and Blending Methods. *Polymer* **2011**, *52*, 1837−1846.
(48) Rafiee, M. A.; Rafiee, J.; Wang, Z.; Song, H.; Yu, Z. Z.; Koratkar, N. Enhanced Mechanical Properties of Nanocomposites at Low Graphene Content. *ACS Nano* **2009**, *3*, 3884−3890.
(49) Kim, H.; Abdala, A. A.; MacOsko, C. W. Graphene/polymer Nanocomposites. *Macromolecules* **2010**, *43*, 6515−6530.
(50) Nguyen, D. A.; Lee, Y. R.; Raghu, A. V.; Jeong, H. M.; Shin, C. M.; Kim, B. K. Morphological and Physical Properties of a Thermoplastic Polyurethane Reinforced with Functionalized Graphene Sheet. *Polym. Int.* **2009**, *58*, 412−417.
(51) El Achaby, M.; Qaiss, A. Processing and Properties of Polyethylene Reinforced by Graphene Nanosheets and Carbon Nanotubes. *Mater. Eng.* **2013**, *44*, 81−89.
(52) Meng, J.; Tajaddod, N.; Cranford, S. W.; Minus, M. L. Polyethylene-Assisted Exfoliation of Hexagonal Boron Nitride in Composite Fibers: A Combined Experimental and Computational Study. *Macromol. Chem. Phys.* **2015**, *216*, 847−855.
(53) Golberg, D.; Bando, Y.; Huang, Y.; Terao, T.; Mitome, M.; Tang, C.; Zhi, C. Boron Nitride Nanotubes and Nanosheets. *ACS Nano* **2010**, *4*, 2979−2993.
(54) Lin, Y.; Connell, J. W. Advances in 2D Boron Nitride Nanostructures: Nanosheets, Nanoribbons, Nanomeshes, and Hybrids with Graphene. *Nanoscale* **2012**, *4*, 6908−6939.
(55) Reina, A.; Jia, X.; Ho, J.; Nezich, D.; Son, H.; Bulovic, V.; Dresselhaus, M. S.; Kong, J. Large Area, Few-Layer Graphene Films on Arbitrary Substrates by Chemical Vapor Deposition. *Nano Lett.* **2009**, *9*, 30−35.
(56) Jiang, J.-W.; Zhao, J.; Zhou, K.; Rabczuk, T. Superior Thermal Conductivity and Extremely High Mechanical Strength in Polyethylene Chains from Ab Initio Calculation. *J. Appl. Phys.* **2012**, *111*, 124304.
(57) Awasthi, A. P.; Lagoudas, D. C.; Hammerand, D. C. Modeling of Graphene−polymer Interfacial Mechanical Behavior Using Molecular Dynamics. *Modell. Simul. Mater. Sci. Eng.* **2009**, *17*, 15002.
(58) Bunn, C. W. The Crystal Structure of Long-Chain Normal Paraffin Hydrocarbons. The "shape" of The< CH2 Group. *Trans. Faraday Soc.* **1939**, *35*, 482−491.
(59) Yang, J.; Huang, Y.; Lv, Y.; Li, S.; Yang, Q.; Li, G. The Synergistic Mechanism of Thermally Reduced Graphene Oxide and Antioxidant in Improving the Thermo-Oxidative Stability of Polypropylene. *Carbon* **2015**, *89*, 340−349.
(60) Dao, T. D.; Jeong, H. M. Graphene Prepared by Thermal Reduction−exfoliation of Graphite Oxide: Effect of Raw Graphite Particle Size on the Properties of Graphite Oxide and Graphene. *Mater. Res. Bull.* **2015**, *70*, 651−657.
(61) Dickinson, L. R.; Kranbuehl, D. E.; Schniepp, H. C. Assessing Graphene Oxide/polymer Interfacial Interactions by Way of Peeling Test. *Surf. Innovations* **2016**, *4*, 158−166.
(62) Duplock, E. J.; Scheffler, M.; Lindan, P. J. D. Hallmark of Perfect Graphene. *Phys. Rev. Lett.* **2004**, *92*, 225502−1.
(63) McAllister, M. J.; Li, J. L.; Adamson, D. H.; Schniepp, H. C.; Abdala, A. A.; Liu, J.; Herrera-Alonso, M.; Milius, D. L.; Car, R.; Prud'homme, R. K.; Aksay, I. A. Single Sheet Functionalized Graphene by Oxidation and Thermal Expansion of Graphite. *Chem. Mater.* **2007**, *19*, 4396−4404.
(64) Schniepp, H. C.; Li, J. L.; McAllister, M. J.; Sai, H.; Herrera-Alonson, M.; Adamson, D. H.; Prud'homme, R. K.; Car, R.; Seville, D. A.; Aksay, I. A. Functionalized Single Graphene Sheets Derived from Splitting Graphite Oxide. *J. Phys. Chem. B* **2006**, *110*, 8535−8539.
(65) Ramanathan, T.; Abdala, A. A.; Stankovich, S.; Dikin, D. A.; Herrera-Alonso, M.; Piner, R. D.; Adamson, D. H.; Schniepp, H. C.; Chen, X.; Ruoff, R. S. Functionalized Graphene Sheets for Polymer Nanocomposites. *Nat. Nanotechnol.* **2008**, *3*, 327.
(66) Menyhárd, A.; Suba, P.; László, Z.; Fekete, H. M.; Mester, O.; Horváth, Z.; Vörös, G.; Varga, J.; Móczó, J. Direct Correlation between Modulus and the Crystalline Structure in Isotactic Polypropylene. *eXPRESS Polym. Lett.* **2015**, *9*, 308−320.
(67) Shen, S.; Henry, A.; Tong, J.; Zheng, R.; Chen, G. Polyethylene Nanofibres with Very High Thermal Conductivities. *Nat. Nanotechnol.* **2010**, *5*, 251−255.
(68) Guo, Z.; Lee, D.; Liu, Y.; Sun, F.; Sliwinski, A.; Gao, H.; Burns, P. C.; Huang, L.; Luo, T. Tuning the Thermal Conductivity of Solar Cell Polymers through Side Chain Engineering. *Phys. Chem. Chem. Phys.* **2014**, *16*, 7764−7771.
(69) Cheng, S.; Chen, X.; Hsuan, Y. G.; Li, C. Y. Reduced Graphene Oxide-Induced Polyethylene Crystallization in Solution and Nanocomposites. *Macromolecules* **2012**, *45*, 993−1000.
(70) Minus, M. L.; Chae, H. G.; Kumar, S. Observations on Solution Crystallization of Poly (Vinyl Alcohol) in the Presence of Single-Wall Carbon Nanotubes. *Macromol. Rapid Commun.* **2010**, *31*, 310−316.
(71) Minus, M. L.; Chae, H. G.; Kumar, S. Single Wall Carbon Nanotube Templated Oriented Crystallization of Poly (Vinyl Alcohol). *Polymer* **2006**, *47*, 3705−3710.
(72) Lei, F.; Yu, H.; Yang, S.; Sun, H.; Li, J.; Guo, S.; Wu, H.; Shen, J.; Chen, R.; Xiong, Y. Analysis of Crystalline Structure and Morphology of Isotactic Polypropylene under the Coexistence of Organic Montmorillonite Particles and Shear Flow. *Polymer* **2016**, *82*, 274−284.
(73) Su, R.; Wang, K.; Zhang, Q.; Chen, F.; Fu, Q.; Xu, W.; Na, B. Orientation and Epitaxy in the Injection-Molded Bars of Linear Low-Density Polyethylene/Isotactic Polypropylene Blends: An Infrared Dichroism Measurement. *J. Phys. Chem. B* **2009**, *113*, 7423−7429.
(74) Zhang, X.; Ajji, A.; Jean-Marie, V. Processing-Structure-Properties Relationship of Multilayer Films. 1. Structure Characterization. *Polymer* **2001**, *42*, 8179−8195.
(75) Guan, Q.; Shen, K.; Ji, J.; Zhu, J. Structure and Properties of Self-reinforced Polyethylene Prepared by Oscillating Packing Injection Molding under Low Pressure. *J. Appl. Polym. Sci.* **1995**, *55*, 1797−1804.
(76) Steurer, P.; Wissert, R.; Thomann, R.; Mülhaupt, R. Functionalized Graphenes and Thermoplastic Nanocomposites Based upon Expanded Graphite Oxide. *Macromol. Rapid Commun.* **2009**, *30*, 316−327.
(77) Jr Hummers, W. S.; Offeman, R. E. Preparation of Graphitic Oxide. *J. Am. Chem. Soc.* **1958**, *80*, 1339.
(78) Pérez-Rigueiro, J.; Viney, C.; Llorca, J.; Elices, M. Silkworm Silk as an Engineering Material. *J. Appl. Polym. Sci.* **1998**, *70*, 2439−2447.
(79) Tersoff, J. Modeling Solid-State Chemistry: Interatomic Potentials for Multicomponent Systems. *Phys. Rev. B: Condens. Matter Mater. Phys.* **1989**, *39*, 5566−5568.
(80) Yang, J.; Pang, Y.; Huang, W.; Shaw, S. K.; Schiffbauer, J.; Pillers, M. A.; Mu, X.; Luo, S.; Zhang, T.; Huang, Y.; Li, G.; Ptasinska, S.; Lieberman, M.; Luo, T. Functionalized Graphene Enables Highly Efficient Solar Thermal Steam Generation. *ACS Nano* **2017**, *11*, 5510−5518.
(81) Sun, H. COMPASS: An Ab Initio Force-Field Optimized for Condensed-Phase Applications Overview with Details on Alkane and Benzene Compounds. *J. Phys. Chem. B* **1998**, *102*, 7338−7364.
(82) Chen, X. P.; Yuan, C. A.; Wong, C. K. Y.; Koh, S. W.; Zhang, G. Q. Validation of Forcefields in Predicting the Physical and Thermophysical Properties of Emeraldine Base Polyaniline. *Mol. Simul.* **2011**, *37*, 990−996.
(83) Luo, T.; Lloyd, J. R. Enhancement of Thermal Energy Transport across Graphene/graphite and Polymer Interfaces: A Molecular Dynamics Study. *Adv. Funct. Mater.* **2012**, *22*, 2495−2502.
(84) Krishnaswamy, R. K.; Janzen, J. Exploiting Refractometry to Estimate the Density of Polyethylene: The Lorentz-Lorenz Approach Re-Visited. *Polym. Test.* **2005**, *24*, 762−765.



DOI: 10.1021/acsnano.8b04734
*ACS Nano* 2019, 13, 1097−1106